Available online at www.sciencedirect.com
SCIENCE DIRECT®
International Journal of Heat and Mass Transfer 47 (2004) 1053–1067
International Journal of HEAT and MASS TRANSFER
www.elsevier.com/locate/ijhmt

Bubble growth on an impulsively powered microheater

Z. Yin [a], A. Prosperetti [a,b,*], J. Kim [c]

[a] Department of Mechanical Engineering, The Johns Hopkins University, Baltimore, MD 21218, USA
[b] Faculty of Applied Physics, Twente Institute of Mechanics, and Burgerscentrum, University of Twente, AE 7500 Enschede, The Netherlands
[c] Department of Mechanical Engineering, University of Maryland, College Park, MD 20742, USA

Received 28 February 2003; received in revised form 25 July 2003

Abstract

The dynamics of single vapor bubbles in FC-72 generated by a transient heat pulse applied to a square 260×260 μm^2 microheater are investigated for different heat fluxes between 3 and 44 MW/m^2. It is found that in all cases the growth consists of two steps, a first relatively violent one, followed by a shrinking of the vapor mass and a subsequent slower expansion. At the higher heat fluxes, the initial growth takes the form of a thin vapor layer, and it is only at the end of the second phase that the bubble acquires a significant size in the direction normal to the heater. At low heat fluxes, on the other hand, the three-dimensional character is apparent from the very beginning. The air dissolved in the liquid diffuses into the bubble during its growth and significantly slows down its shrinking after the end of the heating phase.

1. Introduction

The thermal ink-jet printer has been the first widespread technological application of bubbles in microfluidic devices, and several papers have been devoted to its study [1–5]. More recently, the potential use of bubbles for other applications has begun to be appreciated: actuation [6–8], pumping [9–12], mixing [13], and others.

In many of these applications, one deals with vapor bubbles which are nucleated by impulsive heating, grow, and collapse after the heating stops and the vapor condenses. In many respects, the process is thus quite different from that prevailing in normal boiling conditions, where the heater operates continuously and a nominally steady state is established (see e.g. Refs. [14,15]). These differences have motivated several investigations directed at the study the peculiarities of bubble dynamics under impulsive heating. Okuyama and Iida [16] studied bubble formation on a 100 μm platinum wire in liquid nitrogen. Iida et al. [5,17] used a platinum–chromium planar heater in ethyl alcohol with heating rates close to 10^8 K/s. A transition between a nucleation mechanism similar to that of normal boiling and a different mode, in which many very small bubbles simultaneously appear on the heating surface, was observed.

Similar experiments on a 100×110 μm^2 planar heater and on a 10 μm diameter platinum wire were conducted by Zhao et al. [18] and Glod et al. [19] who, in an effort to gain further insight into the process of liquid heating and bubble formation, monitored the pressure pulse radiated in the liquid by the developing vapor bubbles. The authors attribute the initial vapor formation to thermodynamic fluctuations similar to those responsible for homogeneous nucleation [14,20]. They find that this initial bubble quickly condenses, and is immediately followed by a second phase of vapor growth, characterized by a pressure pulse which can be larger than the one emitted by the initial growth.

The experiments described in the present paper are similar to those of Ref. [18], with differences in the planar heater used, the heating time, and, more importantly, in the physical properties of the liquid, FC-72 rather than water as in their study. We find marked changes in the bubble dynamics as the heat flux is varied

* Corresponding author. Address: Department of Mechanical Engineering, The Johns Hopkins University, Baltimore, MD 21218, USA. Tel.: +1-410-516-8534; fax: +1-410-516-7254.
E-mail addresses: zzyin@titan.me.jhu.edu (Z. Yin), prosperetti@jhu.edu (A. Prosperetti), kimjh@eng.umd.edu (J. Kim).

0017-9310/$ - see front matter © 2003 Elsevier Ltd. All rights reserved.
doi:10.1016/j.ijheatmasstransfer.2003.07.015

Nomenclature

D	thermal diffusivity	r	radius
k	thermal conductivity	R	electrical resistance
p	pressure	t	time
q	heater heat flux	T	temperature

from about 3 to 44 MW/m^2, although in all cases the process consists of two phases similar to the observations reported in Ref. [18].

2. Experiment

The set-up for this experiment is shown in Fig. 1. A cylindrical acrylic chamber, 73 mm inner diameter and 55 mm high, is partially filled with liquid FC-72 (3M Corporation), the relevant physical properties of which can be found at [21]. An array of 96 platinum heaters on a transparent fused quartz substrate is mounted on a PC board which constitutes the bottom of the cell. The platinum layer is about 200 nm thick, and is deposited on a thin layer of Ti which helps bonding with the quartz. The manufacturing and detailed characteristics of this array are described in detail elsewhere [22,23]. Each heater consists of 5 μm wide lines laid out in a serpentine pattern over an area of 260×260 μm^2 (see e.g. the first frame of Fig. 3), with each line 5 μm apart from its neighbor so that the metal covers 50% of the area. The platinum lines were protected by a 1 μm thick SiO_2 layer.

Only one heater of this array was used for the observations reported here, the electrical resistance of which was measured to be 737 Ω at 25 °C. The heater was powered by an amplifier driven by a function generator which produced square dc pulses. The heater was part of an electrical bridge arrangement which facilitated the measurement of the voltage across it. The current through the heater was measured by means of a resistor constituting one element of the bridge and connected in series with it. The magnitude of this resistance ranged from 60 to 100 Ω, adjusted depending on the applied voltage. Voltages were acquired by a NIDAQ AT-MIO-16E-10 board at a rate of 100 kHz.

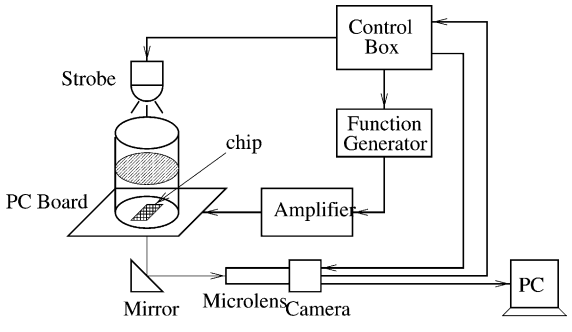

Fig. 1. The experimental set-up.

The average temperature T of the heater was determined by resistance thermometry assuming a linear dependence:

$$\frac{R}{R_0} = 1 + \alpha(T - T_0). \tag{1}$$

The temperature coefficient was found to be $\alpha = 0.00196 \pm 0.00006$ °C^{-1} by measuring the resistance of several heaters on the chip in a temperature-controlled chamber between the temperatures of 40 and 120 °C. While this range is smaller than the temperatures reached in the experiment, it is known that the resistivity of platinum is very close to linear over a wide range (see e.g. Ref. [24, p. 145]), and, therefore it is likely that the extrapolation of (1) over the range of present interest is sufficiently accurate.

A Redlake Megaplus ES4.0 camera, with $2k\times2k$ pixels, was used to capture pictures through a 4.5× microlens. With the arrangement used, the spatial resolution of the camera was about 1.1 μm per pixel. The light source was a Strobotac 1538A strobe. In order to have a sufficient light intensity, it was necessary to use a flash duration of 3 μs, which caused some blurring of the images. The delay time between the start of the heating and the light flash was measured initially by means of a photodiode with an accuracy of ±20 μs. Since the framing rate of the camera was insufficient to capture a sequence of frames from a single event, we took photos of different events by using a control box to vary this delay. Some comments on the degree of reproducibility of the process will be found below. In general, the shot-to-shot variability was greater at the lower heat fluxes.

3. Observations

All the observations described were carried out on the same heater. We have performed tests applying voltages across the bridge from 15 to 55 V in steps of 5 V. We will mainly focus on observations made at low (15 V), intermediate (30 V), and high (50 V) voltages.

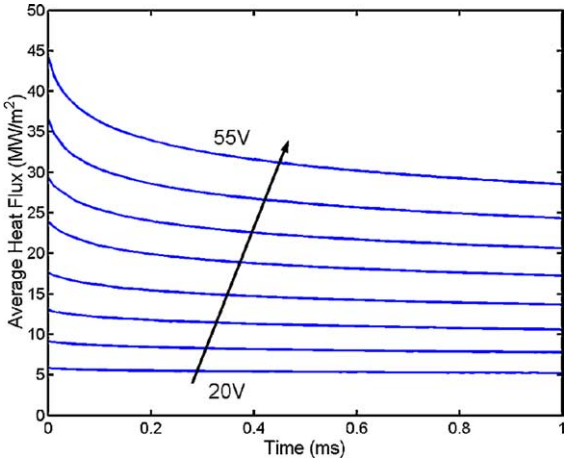

Fig. 2. Average heat flux vs. time for applied voltages of 20–55 V, in steps of 5 V, in ascending order.

Table 1
Summary of the experimental conditions in the present study

Voltage (V)	Average heat flux (MW/m^2)		Heating time (μs)	Figure number
	Initial	At end of heating		
15	3.43	2.92	10,000	3, 4
20	5.85	5.24	1000	
25	9.17	7.78	1000	
30	13.0	10.6	1000	13a–c
35	17.6	13.7	1000	15
40	23.9	17.3	1000	
45	28.3	20.7	1000	
50	36.7	24.3	1000	7a–c, 8
55	44.4	28.5	1000	
55	44.4	38.5	50	16

Since the voltage across the bridge was kept constant, due to the temperature dependence of the heater resistance, the heat flux at the heater changes with time as shown, for different voltages, in Fig. 2. Table 1 lists voltages, heat fluxes and durations of the heating period.

Due to the small thermal diffusivity of the liquid (3.08×10^{-8} m^2/s at 25°, with a specific heat of 1100 J/kg K, a density of 1680 kg/m^3, and a thermal conductivity of 0.057 W/mK) with respect to the underlying quartz (0.308×10^{-7} vs. 9.50×10^{-7} m^2/s; thermal conductivities 0.057 and 1.4 W/mK, respectively, all at 25 °C), most of the heat supplied by the heater diffuses in the quartz rather than in the FC-72; in this respect our situation is similar to that described in Ref. [25].

3.1. Low heat flux

Fig. 3 shows several images taken under conditions of low heating with a voltage of 15 V applied for 10 ms. The corresponding initial heat flux (averaged over the nominal heater area of 260×260 μm^2) was 3.43 MW/m^2. Due to the temperature dependence of the resistance, at the end of the heating period after 10 ms, this heat flux decreased to 2.92 MW/m^2.

Under these conditions, the bubble consistently nucleated near the center of the heater, most likely because this is the position of the maximum temperature (see Fig. 6). At this low power, the system needs a relatively long time before the temperature is high enough to nucleate a bubble. The precise instant at which nucleation takes place varies by a few tens of microseconds from shot to shot, but generally occurs around 3.90 ms after the heater is first powered. Fig. 4 shows examples of bubbles produced by different nucleation events at $t = 3.92$ (upper row) and 4 ms. There are differences in the first set, for which the bubble is very close to the instant of nucleation which, however, are already much reduced by 4 ms.

The first few images of Fig. 3 show that the initial growth of the bubble is very rapid, nearly explosive. By comparing with the known size of the heater, the maximum diameters can be estimated to be of the order of 490 μm. These maximum sizes are well beyond what can be supported by the power supplied by the heater, another indication of the strongly dynamical nature of the initial growth phase. The images corresponding to $t = 5$, 6, and 7 ms in Fig. 3 show the bubble growing from a minimum size attained sometime between $t = 4$ and 5 ms, until it stabilizes over the heater surface for the last 2–3 ms of heating. This stabilization in spite of the fact that, most likely, vapor is condensing at the bubble top, implies that continuous evaporation occurs at the base. It may be expected that strong Marangoni flows are active during this phase of the process.

The last frame in Fig. 3 shows the bubble 5 ms after cessation of the heating. We show later other examples of this phase of the bubble life (Figs. 7c and 13c), and comment on it in connection with Fig. 14.

The average temperature vs. time, deduced from the measured resistance by means of Eq. (1), is shown by the solid line (left scale) in Fig. 5, where the dotted line (to be read on the right scale) is the measured average heat flux. The marked deviations from a monotonic rise of the temperature and decay of the heat flux visible between $t = 4$ and 5 ms correspond to the time at which the bubble attains its minimum size before starting its second growth. The presence of this effect indicates that this phase-change process takes place well below the critical point (178.5 °C), where latent heat is still significant.

The second and third images in Fig. 3 and the second image in the first row of Fig. 4 show a characteristic ring structure, which we interpret as a hemispherical bubble resting on a thin vapor layer. This hypothesis is

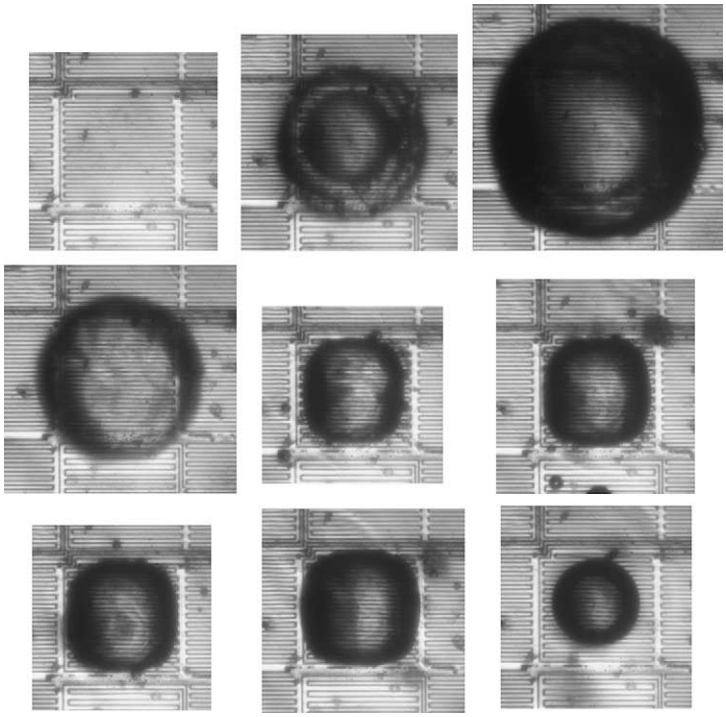

Fig. 3. Typical sequence of bubble behavior for a voltage of 15 V, corresponding to an initial average heat flux of 3.43 MW/m^2. Top row: $t = 3.90$, 3.92, and 3.95 ms; center row: $t = 4$, 5, and 6 ms; bottom row $t = 7$, 10, and 15 ms. The heater is on from $t = 0$ to $t = 10$ ms.

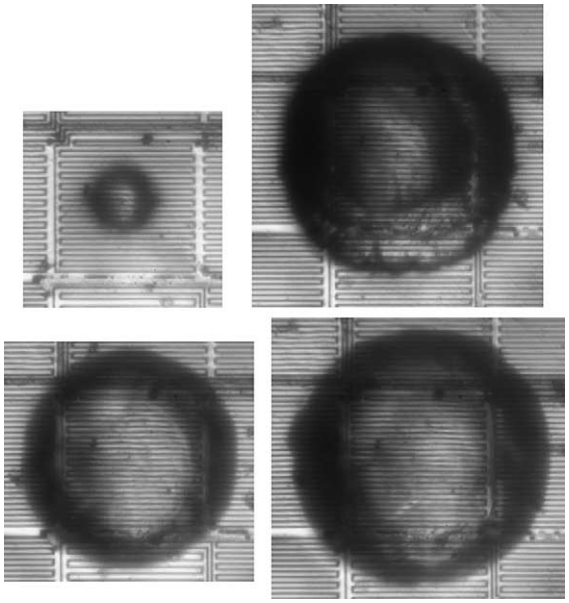

Fig. 4. Images of two different nucleation events at $t = 3920$ μs (upper row) and at $t = 4000$ μs. From the degree of blurring of the first image one may estimate a velocity of the bubble interface of the order of 10 m/s, somewhat lower than the 17 m/s reported in Ref. [18], where however the liquid used was water.

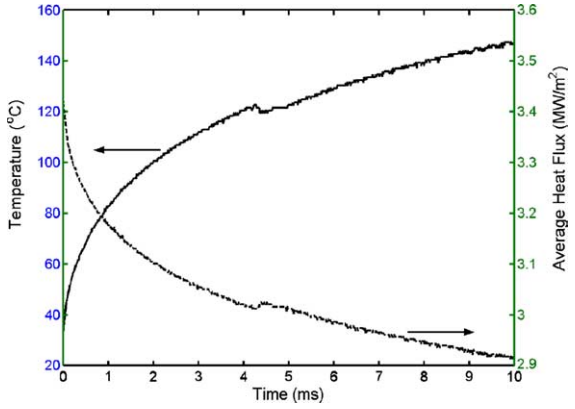

Fig. 5. Average heater temperature (deduced from the measured resistance) and average heat flux vs. time for the low-heat-flux case, 15 V, applied for 10 ms. The initial and final heat fluxes are 3.43 and 2.92 MW/m^2.

supported by the other results shown below e.g. in Fig. 13a. A similar observation was reported in Ref. [26].

The results of Fig. 5 indicate that, at the time of nucleation, the average heater temperature is about 64 °C above the liquid normal boiling point (at which temperature, 120 °C, the latent heat is 64 kJ/kg). In

order to test the reliability of the temperature inferred from the variation of the heater resistance, it is useful to consider a numerical simulation of the heating process.

The thermal diffusion length in the first 4 ms of heating time can be estimated as $\sqrt{Dt} \simeq 62$ μm, where for D we have taken the thermal diffusivity of quartz, since it is over 30 times larger than that of the liquid. On the basis of this estimate, one may rule out significant temperature differences between a heated strip and the adjacent unheated ones (this expectation is borne out by the results shown later in Fig. 10 and the relative analysis). Thus, in order to estimate the heater temperature at the time of nucleation, we solve the heat diffusion equation

$$\frac{\partial T}{\partial t} = D\nabla^2 T, \tag{2}$$

where the thermal diffusivity D, taken as $D^+ = 3.08 \times 10^{-8}$ m^2/s in the upper medium (the liquid) and $D^- = 9.50 \times 10^{-7}$ m^2/s in the lower one, is assumed constant. For simplicity, we assume axial symmetry, with the heater taken to be a disk with the same area as the actual square heater. The initial condition is $T(t=0) = T_0$; at the interface, the temperature is continuous, while the heat fluxes satisfy

$$-k^+\mathbf{n}\cdot\nabla T^+ + k^-\mathbf{n}\cdot\nabla T^- = \begin{cases} q & \text{over the heater} \\ 0 & \text{elsewhere} \end{cases} \tag{3}$$

with $\mathbf{n}$ the unit normal directed from the solid into the liquid, $k^\pm$ the thermal conductivities (again taken as constants, 0.057 and 1.4 W/mK, respectively), and q a constant heat flux switched on at $t = 0+$. The problem was solved by finite differences over a cylindrical domain with a radius of 733.5 μm (five times that of the heater), and heights of 10 times the diffusion lengths during 3.92 ms, namely 110 μm in the liquid and 610 μm in the solid; on the boundaries, the temperature was assumed to be equal to the undisturbed value. Grids of 125×125 nodes were used in each medium, with a time step of 2.45 μs; numerical convergence was tested by varying the number of nodes and the time step. The temperature at the center of the heater as obtained from this finite-difference calculation is shown as a function of time in the upper panel of Fig. 6. These results have been obtained with a heat flux $q = 3.15$ MW/m^2, which is close to the average of the measured heat fluxes at the beginning and at the end of the time interval simulated. It should be kept in mind that Fig. 6 shows the center temperature, while the data of Fig. 5 are for the average temperature. The calculated temperature distribution over the heater at $t = 3.92$ μs is shown in Fig. 6, and exhibits a 56 °C difference between the center and the edge of the heater, with an average of about 125°, which compares very favorably with the measured value of Fig. 5. Thus, we may conclude that the numerical simulations support

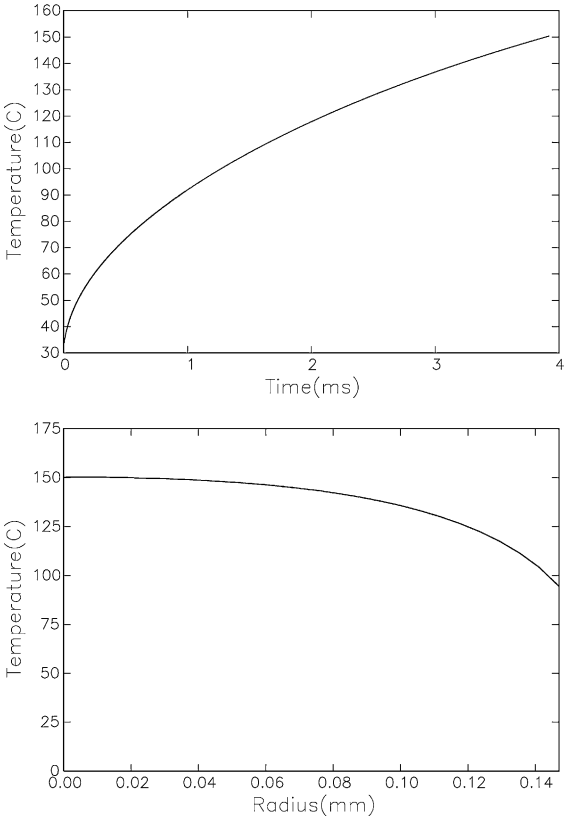

Fig. 6. The upper panel shows the calculated temperature at the center of the heater vs. time from the finite-difference solution of (2) and (3). The lower panel is the temperature distribution over the heater at the nucleation time $t = 3.92$ ms as found from the finite-difference solution of (2) and (3).

the high superheat implied by the resistance data of Fig. 5. In a series of tests with FC-72 in quasi-steady conditions, You et al. [27] found a large scatter in the wall superheat necessary for nucleation and measured superheats up to 50.5 °C. Our conditions are highly transient, which suggests that our superheat, while larger than those of Ref. [27], is not unrealistic.

According to the standard theory of boiling nucleation, the superheat must be high enough that the vapor pressure p_V balance the surface tension overpressure across a hemispherical liquid–vapor interface attached to the mouth of the nucleation site (see e.g. [14]). If the radius of this site is r_n, we thus have

$$r_n = \frac{2\sigma(T_b + \Delta T)}{p_V(T_b + \Delta T) - p_\infty}, \tag{4}$$

where σ is the surface-tension coefficient, T_b the boiling temperature at the ambient pressure p_∞, and ΔT the liquid superheat. With $T_b = 56°$ and $\Delta T = 79$ °C, one finds $p_V = 795$ kPa, $\sigma = 0.00195$ N/m, and $r_n \simeq 6.5$ nm,

to be compared with the minimum value of 24 nm reported by You et al. These very small radii are in keeping with the highly wetting behavior of FC-72 and the nearly molecular smoothness produced by the vapor deposition process with which the heaters were fabricated.

3.2. High heat flux

In the next situation we consider, the applied voltage was 50 V, corresponding to an initial surface-averaged heat flux of 36.7 MW/m^2, which declines to 24.3 MW/m^2 at $t = 1$ ms; now the process is much faster and the heating only lasts 1 ms. Fig. 7a–c show a sequence of images for this case. The first striking difference with the previous case is the nucleation behavior, visible in Fig. 7a, which not only occurs much earlier—between 20 and 30 μs rather than between 3900 and 3920 μs as in the previous case—but also apparently nearly simultaneously at a large number of sites on the heater surface. A similar difference between nucleation at low and high heating rates has been observed by Iida et al. [5,17], who refer to the nucleation pattern in the latter case as "caviarwise nucleation". The nucleation process is also much more repeatable than before: Fig. 8 shows images of different events taken at $t = 30$ and 40 μs, which all show essentially the same behavior.

The images for $t = 30$ and 40 μs in Fig. 7a and those in Fig. 8 show a horizontal band near the lower part of the heater, which is probably due to some non-uniformity in the resistance of the platinum layer. The effects of this non-uniformity appear more clearly later. The upper part of the heater is covered by a large vapor patch. From the fact that the light intensity in this area is fairly uniform, we deduce (see below) that this vapor mass is thin and of a fairly uniform thickness. The frames in the second and third rows of Fig. 7a show that this vapor area shrinks from the sides and gives rise to a (darker and, therefore) more three-dimensional gas–vapor volume near the center of the heater. The irregular shape of the vapor boundary during this phase is similar to the well-known instability of the collapse of a spherical bubble (see e.g. Ref. [28]): the convergence of the flow responsible for the instability in three dimensions is also present, if in a weaker form, in two. The inability of this initial bubble to support itself is probably due to the combined effect of condensation at the top, where the liquid has been in contact with the heater only for less than 30 μs, and is therefore relatively cold, and to the fact that the heater is temporarily dry and unable to supply additional vapor. The heater, however, is still hot and, when liquid wets it again, additional vapor is generated. Unlike the earlier one, since vapor is already present, this phase-change process is not explosive but gradual. Indeed, the last frame of Fig. 7a and the frames in the first row of Fig. 7b show that a contact line expands outward toward the heater edge. Later, the light intensity near this edge starts decreasing, until most of the heater area turns dark (last row of Fig. 7b).

This evolution of the light intensity indicates the gradual growth of the bubble from an initial shape flattened against the heater, to a curved surface with a height comparable to the size of the base. This interpretation is supported by the results, shown in Fig. 9, of a simple geometrical-optics calculation of the light intensity reaching the base of an axisymmetric bubble with a shape given by

$$\left(\frac{r}{L}\right)^2 + \left(\frac{z}{\beta L}\right)^2 = 1, \tag{5}$$

where L is the radius of the base and, from left to right, $\beta = 2$, 1 and 1/2. For $\beta = 1/2$, the assumed shape is an ellipse flattened against the heater, for $\beta = 1$ it is a semicircle, while, for $\beta = 2$, it is an ellipse twice as high as it is wide. To find this result, each incident ray is deflected at the liquid–vapor interface according to Snell's law. The transmitted light intensity is calculated by assuming that the incident intensity in the bundle of rays between r and $r + \mathrm{d}r$ decreases in inverse proportion to the spreading of the bundle after refraction. The results of this calculation are the normalized by the value on the axis of symmetry $r = 0$. It is clear that, as β increases, less and less light reaches the edges of the heater, thus accounting for the dark region around the periphery of the heater apparent in the photographs. The results for a plane geometry are very similar.

The thermal diffusion length during 30 μs, estimated as before, is about 5.3 μm. Thus, over this initial time period and away from the edges, one may approximate the heater as a series of two-dimensional long thin heated strips separated by unheated regions arranged in a periodic pattern.

The energy equation is the same as Eq. (2) above, with the only difference that the Laplacian is now in two Cartesian dimensions, rather than axially symmetric; the condition on the heat flux is also as in (3), but q must now be found by dividing the total electrical power dissipated by the actual heater area, rather than the gross "footprint" of the heater, as before. In view of the assumed horizontal periodicity in the direction normal to the heater strips, the problem can be solved by an expansion in a Fourier cosine series; details are presented in Appendix A. The two dashed lines in Fig. 10 show the calculated temperature distribution along the liquid–solid interface at $t = 20$ and 30 μs. As expected, there are significant spatial gradients, with a maximum temperature at the center of the heater strips of about 170 and 195 °C, respectively, to be compared with the critical temperature of FC-72 of 178.5 °C. These results

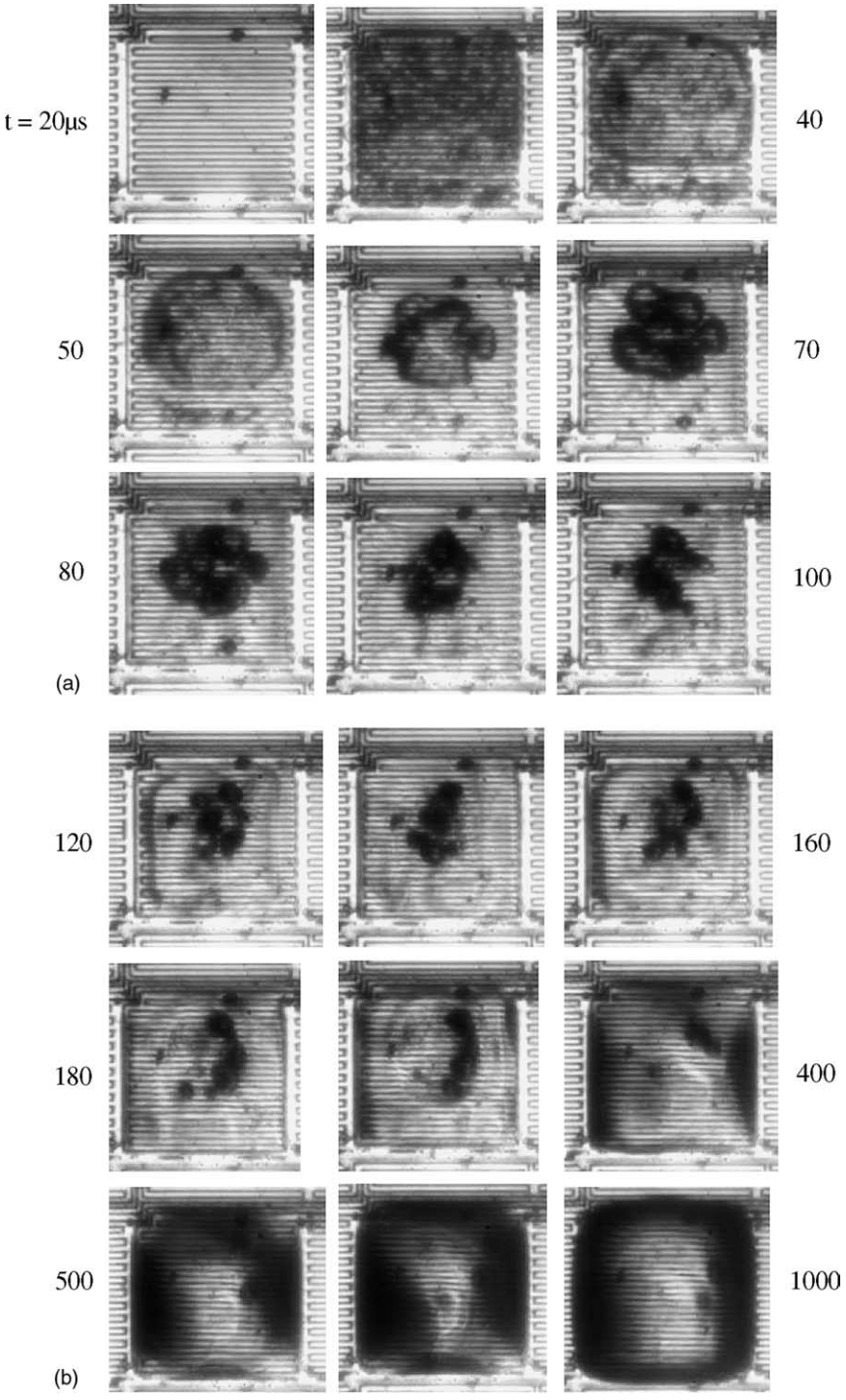

Fig. 7. (a) Early bubble evolution in the high heat flux case, 50 V, $q = 36.7$ MW/m^2. Top row: $t = 20$, 30, and 40 μs; center row: $t = 50$, 60, and 70 μs; bottom row: $t = 80$, 90, and 100 μs. Heating starts at $t = 0$. (b) Later stages of the heating period in the high heat flux case until the heater is switched off at $t = 1000$ μs. Top row: $t = 120$, 140, and 160 μs; center row: $t = 180$, 200, and 400 μs; bottom row: $t = 500$, 600, and 1000 μs. (c) Evolution of the bubble for the high heat flux case after the heater is turned off. Top row: $t = 2000$, 3000, and 5000 μs; second row: 6000, 8000, and 10,000 μs.

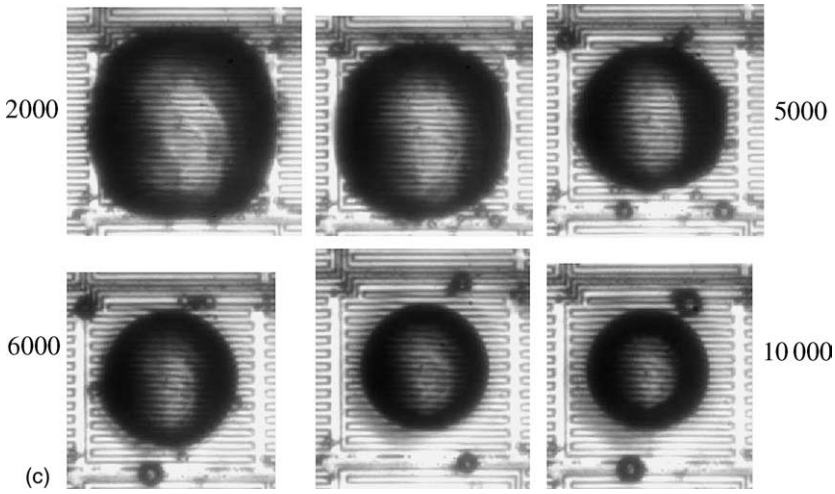

Fig. 7 (*continued*)

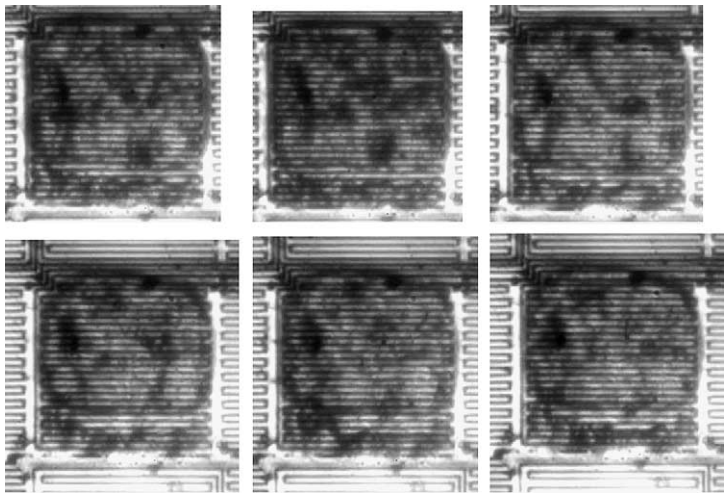

Fig. 8. Three different images of the heater surface at $t = 30$ μs (top row) and $t = 40$ μs for the high heat flux case showing the reproducibility of the nucleation process.

suggest that in this case nucleation occurs very close to the critical temperature, where the latent heat is very small.

From the same analytic solution we can calculate the rate of rise dT/dt of the surface-average and local temperatures. Since in the model we impose a time-independent heat flux q, and $dT/dt \propto q$, it is convenient to plot $(dT/dt)/q$, rather than different diagrams, one for each value of q. The results are shown in Fig. 12, in which the solid line is the surface-average dT/dt, while the dashed line is the value at the center of the heated strip. In this figure the symbols show the experimental results obtained by numerical differentiation of the measured average temperatures of Fig. 11. For the present case (crosses), at the moment of nucleation, with $q = 66.4$ MW/m^2 (the measured value at $t = 30$ μs), one finds $dT/dt = 1.96 \times 10^6$ °C/s.

We were unable to collect temperature data at a rate faster than 100 kHz, and therefore our resolution is not sufficient to ascertain whether there is a significant cooling of the heater at the moment of bubble growth comparable to that shown in Fig. 5 for the low-heat-flux case. The uppermost line in Fig. 11 shows the average heater temperature vs. time for a single event at this power level: in contrast with the previous one only a slight deviation from a smooth behavior can be detected

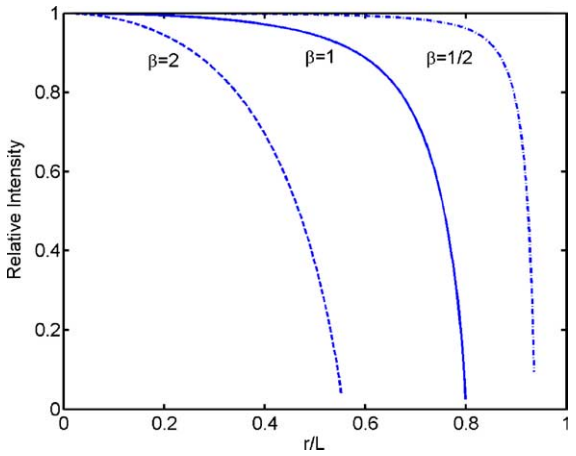

Fig. 9. Geometrical-optics image intensity for uniformly distributed light falling onto an axisymmetric ellipsoidal bubble shape (5). The dash-dot line is for $\beta = 1/2$ (ellipse flattened against the heater), the solid line for $\beta = 1$ (semi-circle), and the dashed line for $\beta = 2$.

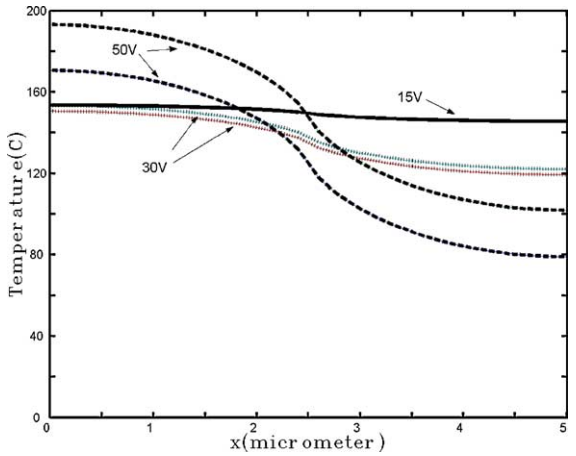

Fig. 10. Calculated temperature distribution over one spatial period of a model heater consisting of alternating heated and unheated strips. Solid line: low heat flux case of Fig. 3 at $t = 3920$ μs; dashed lines: high heat flux case of Fig. 7a–c at $t = 20$ and 30 μs; dotted lines: intermediate heat flux case of Fig. 13a–c at $t = 200$ and 210 μs.

around $t = 10$ μs. This effect is due to a single data point and seemingly occurs before nucleation; it could just be the result of a random fluctuation. No significant cooling is apparent at nucleation around $t = 30$ μs. Some slight unevenness in the rate of temperature growth is present starting at around 60 μs, probably correlated with the secondary vapor growth mentioned before.

After the heater is switched off (Fig. 7c), the bubble becomes more rounded and slowly shrinks as vapor condenses and air diffuses out into the liquid.

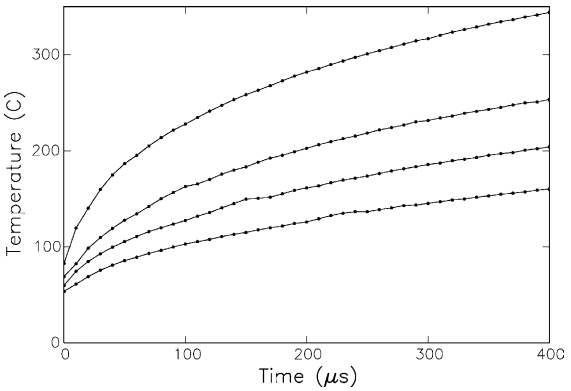

Fig. 11. Average heater temperature (deduced from the measured resistance) vs. time for, in ascending order, 30, 35, 40, and 50 V.

3.3. Intermediate heat flux

The intermediate voltage of 30 V corresponds to an initial surface-averaged heat flux of 13.0 MW/m^2, which declines to 10.6 MW/m^2 when the heater is switched off at $t = 1$ ms. The bubble evolution during the heating period is shown in Fig. 13a and b, and the subsequent shrinking by condensation and diffusion in Fig. 13c.

Several nucleation events occurs between 210 and 220 μs on one (or a few) heater strips near the lower edge of the heater. These initial bubbles grow very rapidly and, judging from the darkness of their image, hemispherically or nearly so. The third image at $t = 230$ (and, if less clearly, also the second one) shows an advancing vapor front which is apparently much thinner and moves to

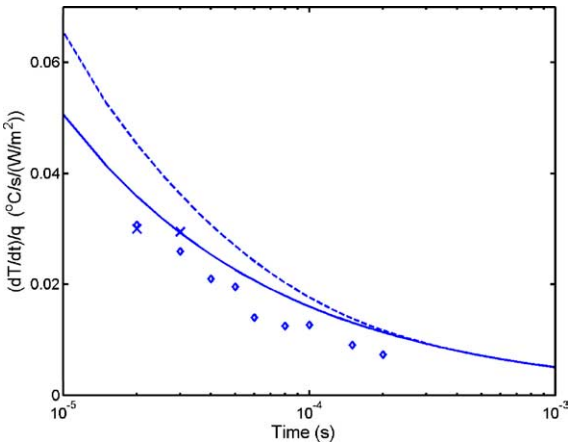

Fig. 12. Calculated derivative of the temperature divided by the imposed heat flux at the center of heated strip (dashed line) and averaged over the spatial period (solid line). The symbols are the measured data: ◇, 30 V, ×, 50 V.

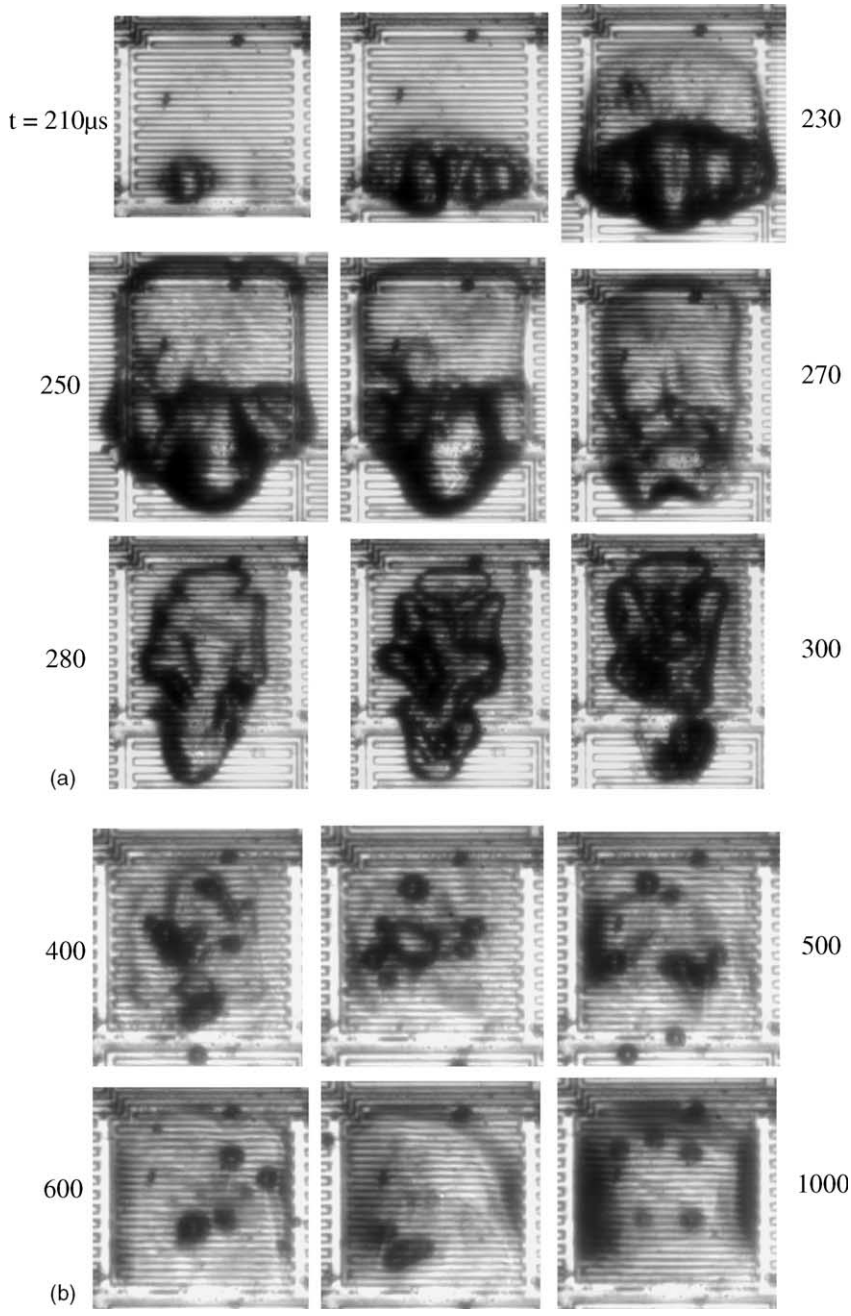

Fig. 13. (a) Bubble evolution during the first part of the heating period in the intermediate heat flux case, 30 V, $q = 13$ MW/m^2. Top row: $t = 210$, 220, and 230 μs; middle row: $t = 250$, 260, and 270 μs; last row: $t = 280$, 290, and 300 μs. Heating starts at $t = 0$. (b) Bubble evolution during the second part of the heating period in the intermediate heat flux case, 30 V, $q = 10.6$–13.0 MW/m^2. Upper row: $t = 400$, 450, and 500 μs; bottom row: $t = 600$, 700, and 1000 μs. (c) Evolution of the bubble for the intermediate heat flux case after the heater is switched off. Top row: $t = 1500$, 2000, and 3000 μs; bottom row: $t = 4000$, 6000, and 9000 μs.

eventually cover the entire heater. This mode of growth is much less dynamic. From the fact that the third, fourth, and fifth frames show some slightly darker spots in the area covered by this vapor, which probably correspond to small bubbles, one may deduce that a liquid microlayer exists under it.

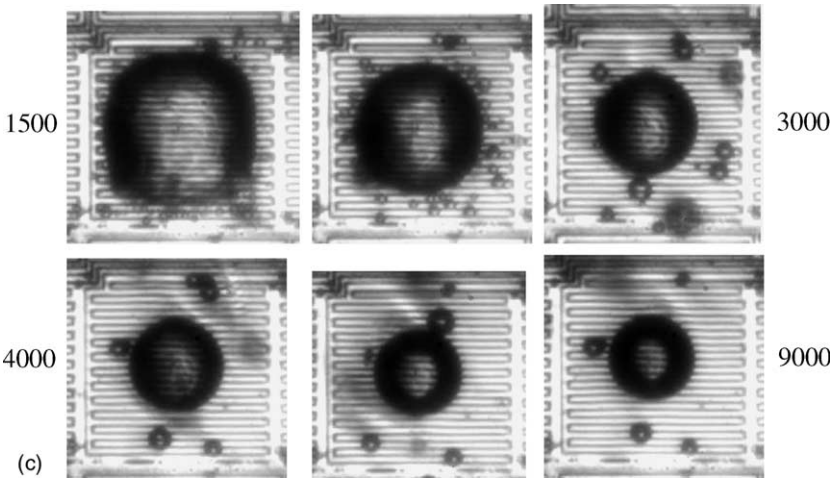

Fig. 13 (*continued*)

Just as in the previous case, the penetration of the vapor into the region of cold liquid causes condensation and the heater is apparently wetted by the liquid again. The first two images of Fig. 13b, for $t = 400$ and 450 μs, show again a liquid–vapor boundary of an irregular, but roughly square shape. This bubble grows to cover the entire heater and protrudes out into the liquid at the end of heating period at $t = 1$ ms (last image of Fig. 13b). After the heater is turned off (Fig. 13c), the process is similar to that seen before in Fig. 7c: the square bubble becomes rounded and gradually shrinks as vapor condenses and air diffuses out.

The lowest line in Fig. 11 is the average heater temperature for this case. There is a clear sign of a faster temperature rise lasting 20–30 μs after the time of nucleation (≈210 μs), followed by a cooling period of about equal duration. From Fig. 13a it can be seen that this period corresponds to vigorous vapor generation.

The results of the analytical calculation of the heater temperature of the Appendix for this case are shown by the dotted lines in Fig. 10 at $t = 200$ and 210 μs. Again one notices a significant spatial non-uniformity; the hottest temperature may be estimated to be around 150 °C at nucleation. The measured data of the surface-averaged dT/dt are shown by the diamonds in Fig. 12; the calculated value for the measured $q = 23.5$ MW/m^2 at the moment of nucleation, $t = 210$ μs, is $dT/dt = 0.33 \times 10^6$ °C/s.

The lowest (dotted) line in Fig. 14 shows the bubble radius vs. the time elapsed after the heater is switched off for the present case of 30 V. It is observed that the radius very nearly stabilizes after an initial decay. This persistence must be attributed to the air dissolved in the liquid, which diffuses into the bubble as long as there is enough vapor pressure to sustain it. As a matter of fact,

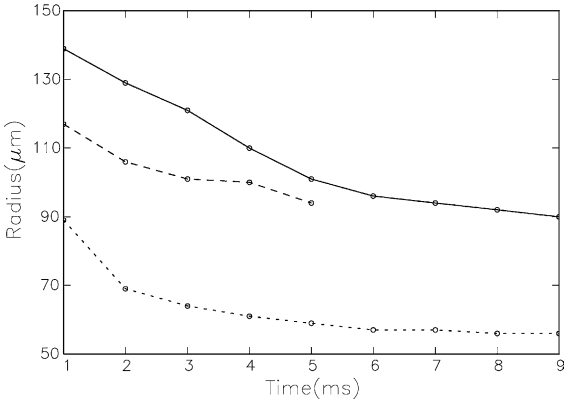

Fig. 14. Bubble radius vs. time elapsed after the termination of the heating for 50 V (solid line), 15 V (dashed line), and 30 V (dotted line). Note that, while for the 30 and 50 V cases the heating duration was 1 ms, it was 10 ms for the 15 V case. This circumstance explains the bigger radius of the bubble in this case.

air is so highly soluble in FC-72 that, at 25 °C, the saturated liquid contains a volume of air equal to 48% of its volume. If the shrinkage of the bubble is entirely attributed to diffusion, a simple calculation following the lines of Ref. [29] shows that a diffusion coefficient of the order of 4×10^{-7} m^2/s would be necessary to match the early part of the data. The diffusion coefficient of nitrogen in FC-72 has recently been measured to be 9.01×10^{-9} m^2/s at 25 °C [30]. The disparity between the two orders of magnitude strongly suggests that the initial shrinkage is due to vapor condensation, while diffusion only sets in later, presumably where the curves flatten after 6–7 ms.

3.4. Other heat fluxes

At 35 V (initial $q = 17.6$ MW/m^2), around $t = 110$ μs, one observes nucleation at several sites in the same lower part of the heater as in the first frame of Fig. 13a, which is followed about 20 μs later by nucleation near the top of the heater (see Fig. 15). This second group of nucleation events occurs at a larger superheat and is, accordingly, more violent. The vapor masses generated by these events are joined by a thinner vapor layer forming by the same mechanism as in frames 3 and 4 of Fig. 13a. As before, these initial large bubbles protrude too far into the cold liquid and quickly condense, leaving only a vapor layer near the heater surface (last frame of Fig. 15).

The second line from the bottom in Fig. 11 shows the measured average heater temperature for this case. We notice the same slight change of concavity upward right around the nucleation time at $t = 110$ observed for 30 V, followed around $t = 160$ μs by a short period during which the temperature undergoes a slight drop, corresponding to the copious formation of vapor visible in

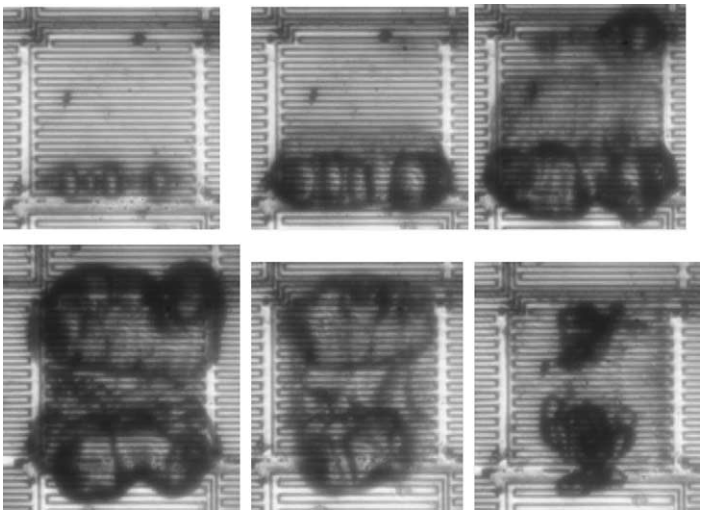

Fig. 15. Bubble evolution for 35 V (initial $q = 17.6$ MW/m^2). Top row: $t = 110$, 120, and 130 μs; bottom row: $t = 140$, 160, and 180 μs. Heating starts at $t = 0$.

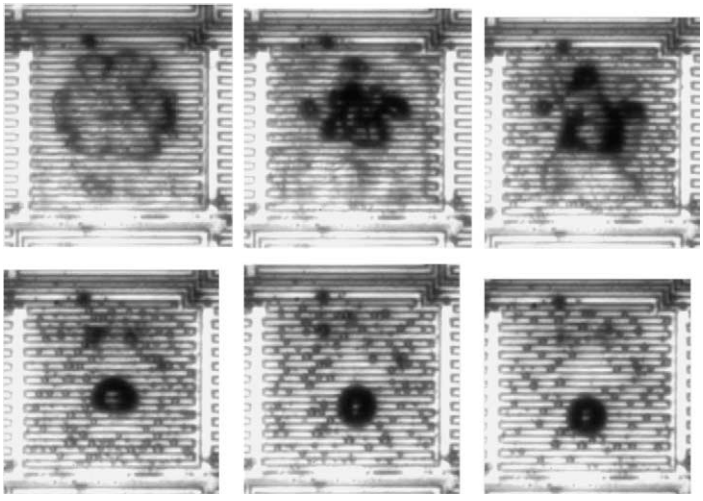

Fig. 16. Bubble evolution for 55 V (initial $q = 44.4$ MW/m^2). Top row: $t = 50$, 100, and 140 μs; bottom row: $t = 300$, 500, and 800 μs. Heating starts at $t = 0$.

the first two frames in the second line of Fig. 15. A similar behavior is observable in the line of Fig. 11 corresponding to 40 V.

Another interesting result is for a high voltage case, 55 V, in which however the heating only lasts 50 μs. Here the initial nucleation occurs around $t = 30$ μs and looks very similar to the second frame of Fig. 7a. At the time the heating stops at $t = 50$ μs the picture (first frame of Fig. 16) is very similar to the $t = 60$ μs image of Fig. 7a. In spite of the fact that the heater has been turned off, there is enough energy left in the substrate to promote a second vapor growth, as seen in the second frame of Fig. 16 for $t = 100$ μs. This secondary vapor however quickly condenses (frames 3 and 4), leaving a central, mostly gas, bubble as before. The notable feature here are the many tiny air bubbles clearly visible in the bottom row of pictures. These are likely due to the dissolved air coming out of solution due to the liquid temperature increase. The difference with the previous cases, where the duration of the heating was much longer, is that this gas had the time to merge with the main bubble.

4. Conclusions

In this paper, vapor bubble growth in FC-72 on a 260×260 μm^2 heater powered for 1–10 ms has been studied for heat flux levels spanning more than one order of magnitude, from 3 to 44 MW/m^2. Marked differences have been observed over this range. At the lower heat fluxes, a single large bubble grows very dynamically overshooting its equilibrium size, shrinks, and then essentially stabilizes over the heater. At higher heat fluxes, nucleation occurs much more repeatably at several spots over the heater. Initially, a vapor volume in the form of a thin layer is formed, which shrinks and is later followed by a more massive vapor growth. While, in the former case, the liquid appears to have stored enough thermal energy to limit the bubble shrinkage after the initial rapid growth, at high heat flux, the nucleation temperature is reached much earlier and there is insufficient time for a substantial mass of liquid to heat up. In these conditions, the heat stored in the solid substrate must play an important role in the secondary vapor growth. This fact is particularly clear at the highest heat flux investigated (Fig. 16), where the second growth occurs after the heater has been turned off. Another contributing factor is probably that, during the final stages of the collapse of the initial vapor mass, the pressure of the vapor–gas mixture in the bubble sharply increases due to compression and the release of latent heat upon condensation, and it is this high pressure which favors a second expansion of the vapor region. A similar two-stage process has been reported by Glod et al. in the case of water both for the case of a planar heater, similar to ours [18], and for a thin wire heater [19]. In this latter case, the vapor pressure increase is probably the dominant effect.

At the lower heat fluxes, the heater surface is found to cool substantially upon the growth of the bubble (Fig. 5), which indicates strong latent heat effects, as one would expect far from the critical point of the liquid. While still noticeable, this cooling is much less marked as the heat flux is increased (Fig. 11) until, above about 25 MW/m^2, it becomes difficult to detect. At the same time, the estimated bubble nucleation temperature increases and becomes closer to the critical temperature.

For the practical applications of the impulsive bubble growth studied here, it is essential to understand the process so as to be able to better control it. While our observations and analysis have shed light on several aspects of the phenomenon, others remain unclear. What is the nature and the mechanism responsible for structures such as those shown in the first line of images in Fig. 7b, in which an inner vapor mass (dark area) is apparently surrounded by another one (as identified by a liquid–vapor contact line)? What is the energetically most efficient heating protocol for a desired bubble size? How can one limit, or suppress, the secondary vapor growth so as to have one stroke per heat pulse? Hopefully, the answer to these and other questions will become clearer as the work progresses.

Acknowledgements

The work of the first two authors (ZY and AP) was supported by NSF under grant CTS-9987765. The last author (JK) acknowledges support by NSF under grant CTS-9818278 and NASA under grant NCC3783.

We are grateful to Mr. Jun Chen, Dr. Xiaofeng Liu, and Prof. Joe Katz (Johns Hopkins University) for allowing us to use their CCD camera system and to Dr. He Yuan for useful discussions.

Appendix A

In order to have an estimate of the temperature distribution over the heater surface in the high-heat flux cases, where the serpentine structure of the heater may be expected to induce significant temperature non-uniformities, we consider a periodic arrangement of long heating strips separated by unheated strips. The assumption of two-dimensionality is justified by the fact that the heater linear dimensions (260 μm) are much larger than the width of each heating strip (5 μm), while that of periodicity rests on the fact that there are many heating strips. The mathematical model is quite similar to the one given before in (2) and (3), with the only differences that now the Laplacian operator has the

two-dimensional form $\nabla^2 T = \partial^2 T/\partial x^2 + \partial^2 T/\partial y^2$, with x and y in the horizontal and vertical directions, respectively, and that the boundary condition at the interface is

$$-k^+ \left.\frac{\partial T}{\partial y}\right|_{y=0+} + k^- \left.\frac{\partial T}{\partial y}\right|_{y=0-} = \begin{cases} q & 0 \leqslant x < \frac{1}{2}L \\ 0 & \frac{1}{2}L < x \leqslant L \end{cases} \tag{A.1}$$

with q a constant heat flux imposed at $t = 0+$. Here and in the following the superscript + refers to the liquid, occupying the region $0 \leqslant y < \infty$, and the superscript − to the solid.

In view of the periodicity boundary conditions, according to which $\partial T/\partial x = 0$ at $x = 0$ and L, we expand the temperature in a Fourier cosine series:

$$T^{\pm} = \frac{1}{2} T_0^{\pm}(y,t) + \sum_{n=1}^{\infty} T_n^{\pm}(y,t) \cos n\pi \frac{x}{L}. \tag{A.2}$$

The coefficients T_n are found to satisfy

$$\frac{\partial T_n^{\pm}}{\partial t} = D\left[\frac{\partial^2 T_n^{\pm}}{\partial y^2} - \left(\frac{n\pi}{L}\right)^2 T_n^{\pm}\right] \quad k = 0, 1, 2, \ldots \tag{A.3}$$

To solve these equations we use the Laplace transform finding

$$\widetilde{T}_n^{\pm} = \frac{\widetilde{A}_n}{s} q_n \exp\left(\mp y \sqrt{\frac{s}{D^{\pm}} + \left(\frac{n\pi}{L}\right)^2} \right) \tag{A.4}$$

in which s is the Laplace variable conjugated to t, tildes denote Laplace-transformed quantities,

$$\widetilde{A}_n^{-1} = k^+ \sqrt{\frac{s}{D^+} + \left(\frac{n\pi}{L}\right)^2} + k^- \sqrt{\frac{s}{D^-} + \left(\frac{n\pi}{L}\right)^2}, \tag{A.5}$$

and

$$q_n = \begin{cases} q & n = 0 \\ 2q/[(2\ell+1)\pi] & n = 2\ell + 1 \\ 0 & n \text{ even} \end{cases} \tag{A.6}$$

The Laplace transforms can be inverted with the results, at $y = 0$,

$$T_0(0,t) = \frac{2q}{\sqrt{\pi}} \frac{\sqrt{D^+ D^- t}}{k^+\sqrt{D^-} + k^-\sqrt{D^+}} \tag{A.7}$$

$$\begin{aligned} T_n(0,t) = {} & \frac{L q_n}{n\pi} \frac{k^+ k^-}{(k^-)^2 - (k^+)^2} \\ & \times \sqrt{\frac{1/D^+ - 1/D^-}{(k^+)^2/D^+ - (k^-)^2/D^-}} \exp(-\beta_n t) \\ & \times \left[\operatorname{erf}\left(\sqrt{\lambda^+ t}\right) - \operatorname{erf}\left(\sqrt{\lambda^- t}\right)\right] + \frac{L}{n\pi} \frac{q_n}{(k^+)^2 - (k^-)^2} \\ & \times \left[k^+ \operatorname{erf}\left(\frac{n\pi}{L}\sqrt{D^+ t}\right) - k^- \operatorname{erf}\left(\frac{n\pi}{L}\sqrt{D^- t}\right)\right] \end{aligned} \tag{A.8}$$

where

$$\beta_n = \frac{(k^+)^2 - (k^-)^2}{(k^+)^2/D^+ - (k^-)^2/D^-} \left(\frac{n\pi}{L}\right)^2 \tag{A.9}$$

$$\lambda^{\pm} = \left[D^{\pm} - \frac{(k^+)^2 - (k^-)^2}{(k^+)^2/D^+ - (k^-)^2/D^-}\right] \left(\frac{n\pi}{L}\right)^2 \tag{A.10}$$

References

[1] R. Allen, J. Meyer, W. Knight, Thermodynamics and hydrodynamics of thermal ink jets, Hewlett–Packard J. 36 (1985) 21–27.

[2] A. Asai, T. Hara, I. Endo, One-dimensional model of bubble growth and liquid flow in bubble jet printers, Jpn. J. Appl. Phys. 26 (1987) 1794–1801.

[3] A. Asai, Bubble dynamics in boiling under high heat flux pulse heating, J. Heat Transfer 113 (1991) 973–979.

[4] R. Burr, S. Berger, D. Tence, Overview of phase change piezoelectric ink jet fluids modeling and design, in: H.e.a. Coleman (Ed.), 1996 Fluids Engineering Conference FED-Vol. 239, vol. 4, ASME, 1996, pp. 545–552.

[5] Y. Iida, K. Okuyama, K. Sakurai, Boiling nucleation on a very small film heater subjected to extremely rapid heating, Int. J. Heat Mass Transfer 37 (1994) 2771–2780.

[6] L. Lin, A. Pisano, Bubble forming on a microline heater, in: D. Cho (Ed.), Micromechanical Sensors, Actuators, and Systems, DSC, vol. 32, ASME, 1991, pp. 147–163.

[7] L. Lin, A. Pisano, Thermal bubble powered microactuators, Microsyst. Technol. J. 1 (1994) 51–58.

[8] A. Papavasiliou, D. Liepmann, A. Pisano, Fabrication of free-floating silicon gate valve, in: A. Lee, L. Lin, F. Forster, Y. Young, K. Goodson, R. Keynton (Eds.), Proceedings of the ASME MEMS Division, 1999 IMECE, vol. 1, ASME, New York, 1999, pp. 435–440.

[9] T. Jun, C. Kim, Microscale pumping with traversing bubbles in microchannels, in: Solid-State Sensor and Actuator Workshop, Transducer Research Foundation, Hilton Head Island, 1996, pp. 144–147, 96TRF-0001.

[10] H. Yuan, A. Prosperetti, The pumping effect of growing and collapsing bubbles in a tube, J. Micromech. Microeng. 9 (1999) 402–413.

[11] E. Ory, H. Yuan, A. Prosperetti, S. Popinet, S. Zaleski, Growth and collapse of a vapor bubble in a narrow tube, Phys. Fluids 12 (2000) 1268–1277.

[12] X. Geng, H. Yuan, H. Oğuz, A. Prosperetti, Bubble-based micropump for electrically conducting liquids, J. Micromech. Microeng. 11 (2001) 270–276.

[13] J. Tsai, L. Lin, Active microfluidic mixer and gas bubble filter driven by thermal bubble micropump, Sens. Actuators, A 97–98 (2002) 665–671.

[14] V.P. Carey, Liquid–Vapor Pahse-Change Phenomena, Taylor & Francis, Washington, 1992.

[15] V. Dhir, Boiling heat transfer, Ann. Rev. Fluid Mech. 30 (1998) 365–402.

[16] K. Okuyama, Y. Iida, Transient boiling heat transfer characteristics of nitrogen (bubble behavior and heat transfer rate at stepwise heat generation), Int. J. Heat Mass Transfer 33 (1990) 2065–2071.

[17] Y. Iida, K. Okuyama, K. Sakurai, Peculiar bubble generation on a film heater submerged in ethyl alcohol and imposed a high heating rate over 10^7 K s^{-1}, Int. J. Heat Mass Transfer 36 (1993) 2699–2701.
[18] Z. Zhao, S. Glod, D. Poulikakos, Pressure and power generation during explosive vaporization on a thin-film microheater, Int. J. Heat Mass Transfer 43 (2000) 281–296.
[19] S. Glod, D. Poulikakos, Z. Zhao, G. Yadigaroglu, An investigation of microscale explosive vaporization of water on an ultrathin Pt wire, Int. J. Heat Mass Transfer 45 (2002) 367–379.
[20] V. Skripov, Metastable Liquids, Wiley, New York, 1974.
[21] http://cms.3m.com/cms/US/en/2-68/iilzRFS/view.jhtml.
[22] T. Rule, J. Kim, Heat transfer behavior on small horizontal heaters during pool boiling of FC-72, J. Heat Transfer 121 (1999) 386–393.
[23] N. Yaddanapudi, J. Kim, Single bubble heat transfer in saturated pool boiling of FC-72, Multiphase Sci. Technol. 12 (2001) 47–63.
[24] T. McGee, Principles and Methods of Temperature Measurement, Wiley, New York, 1988.
[25] K. Fushinobu, T. Nagasaki, T. Saitoh, K. Hijikata, Boiling heat transfer characteristics from very smalll heaters on a substrate, in: G. Hewitt (Ed.), Proceedings of the 10th International Heat Transfer Conference, vol. 6, 1994, pp. 51–56.
[26] J.S. Ervin, H. Merte Jr., R.B. Keller, K. Kirk, Transient pool boiling in microgravity, Int. J. Heat Mass Transfer 35 (1992) 659–674.
[27] S. You, A. Bar-Cohen, T. Simon, Boiling incipience and nucleate boiling heat transfer of highly wetting dielectric fluids from electronic materials, IEEE Trans. Comp. Hybrids Manuf. Technol. 13 (1990) 1032–1039.
[28] Y. Hao, A. Prosperetti, The effect of viscosity on the spherical stability of oscillating gas bubbles, Phys. Fluids 11 (1999) 1309–1317.
[29] M. Plesset, A. Prosperetti, Bubble dynamics and cavitation, Ann. Rev. Fluid Mech. 9 (1977) 145–185.
[30] P. Tuma, 3M Corporation, private communication, 2003.